Spatiotemporal Chaos, Stochasticity and Transport in Toroidal magnetic Configurations

M. Rajković 1), Tomo-Hiko Watanabe 2), M. Škorić 2)

1) Institute of Nuclear Sciences Vinča, Belgrade, Serbia
2) National Institute for Fusion Science, Gifu, Japan

E-mail contact of main author: milanr@vin.bg.ac.rs

Abstract. In order to get a more complete insight into the transport processes, zonal flow dynamics and the nature of stochasticity in toroidal systems (helical and tokamak) we analyze nonlinear gyrokinetic Vlasov simulation (GKV) results for the tokamak and the standard and the inward shifted helical configurations from the aspect of nonlinear dynamic systems theory. In both the tokamak and the helical case we show how stochasticity arises from spatiotemporal chaos (STC) . Reduction of transport in the inward shifted configuration with respect to the standard one is interpreted as a consequence of STC suppression while analogous phenomenon is noticed in the purely temporal behavior of plasma dynamics. Hence, in the helical configuration the inward shifted helical configuration represents means for control of spatiotemporal chaos. Layapunov exponents, evaluated with respect to the complete spatiotemporal dynamics , are shown to be directly related to transport properties.

1. Introduction

Sheared $\mathbf{E} \times \mathbf{B}$ plasma flows possessing toroidal and poloidal symmetries known as zonal flows, have been investigated in numerous theoretical, numerical and experimental studies as one of the main mechanisms regulating turbulent transport in magnetic confinement fusion [1], [2], [3], [4]. Also, $\mathbf{E} \times \mathbf{B}$ shear suppression of turbulence is well known to be directly related to various improved confinement regimes. In toroidal systems, the zonal flow is coupled to the geodesic acoustic mode (GAM) oscillations [5], and it is considered that the residual zonal flow remaining constant after Landau damping of the GAM plays an important role in reduction of tokamak ion temperature gradient (ITG) turbulent transport [1].

The extension of gyrokinetic theory of zonal flows driven by the ITG turbulence to helical systems [6] has shown that a high-level zonal flow can be maintained for a longer time by reducing bounce-averaged radial drift velocity of ripple trapped particles. This opened up a possibility for optimization of helical configuration for reduction of turbulent transport by enhancement of zonal flows. A survey of transport optimization methods in stellarators (toroidal magnetic devices) was presented in [7]. These studies have also presented arguments that there is a close relationship between neoclassical and anomalous transport through generation of zonal flows. Also, recent experiments on the Large Helical Device (LHD) have shown that both the neoclassical and the anomalous transport processes are reduced in the inward-shifted configuration [8]. The inward plasma shift decreases the radial particle drift but increases the unfavorable magnetic curvature which destabilizes pressure-gradient driven instabilities such as ITG modes. Consequently, zonal flow may be maintained for a longer time by reduction of bounce-averaged radial drift velocity of helical-ripple-trapped particles. Such a scenario implies that optimization of magnetic configuration for reduction of neoclassical ripple transport at the same time enhances residual zonal flows which in turn also lower the anomalous transport [6], [7], [9], [10].

The nonlinear gyrokinetic simulation yields results for turbulent ion thermal diffusivity χ_i whose temporal behavior was interpreted as a global indicator of transport properties in two configurations. In the inward-shifted configuration, the ion thermal diffusivity grows faster in the initial state while displaying lower average value at the later time accompanied with stronger zonal flows and causal relationship was deduced between these two phenomena [11], [12].

In order to get a more complete insight into the transport processes and zonal flow dynamics in helical (standard and the inward shifted configurations) and tokamak systems nonlinear gyrokinetic Vlasov simulation (GKV) results are analyzed from the aspect of nonlinear dynamic systems theory [13].

2. Gyrokinetic Model for Helical System

The basic formulae for describing the drift wave turbulence in magnetically-confined plasmas are given by the gyrokinetic equations, where time-evolution of the one-body distribution function is described as a nonlinear partial differential equation defined on the five-dimensional phase space. In the gyrokinetics, the finite gyro-radius effect is introduced while the gyro-phase averaging eliminates the fast time-scale phenomena associated with gyro-motions. The nonlinear gyrokinetic equation of the perturbed gyro-center distribution function δf in the low-β (electrostatic) limit,

$$
\left[\frac{\partial}{\partial t} + v_\parallel \hat{\mathbf{b}} \cdot \nabla + \mathbf{v}_d \cdot \nabla - \mu \left(\hat{\mathbf{b}} \cdot \nabla \right) \frac{\partial}{\partial v_\parallel} \right] \delta f + \frac{c}{B_0} \{ \Phi, \delta f \}
$$
$$
= \left(\mathbf{v}_* - \mathbf{v}_d - v_\parallel \hat{\mathbf{b}} \right) \cdot \frac{e \nabla \Phi}{T} F_M + C(\delta f),
$$

(2.1)

is numerically solved in the GKV code. Here, the parallel velocity $v_\parallel$ and the magnetic moment μ are chosen as velocity-space coordinates, where $\mu \equiv v_\perp^2 / 2\Omega_i$ with the ion cyclotron frequency $\Omega_i = eB / m_i c$. In the expression for Ω_i, m_i is the ion mass and $v_\perp$ is the perpendicular velocity. Each term on the left-hand-side (l.h.s.) of Eq.(2.1), except for the time derivative one, represents advection of δf along gyrocenter orbits in the phase space. The background distribution is approximated by the Maxwellian F_M. The collision term is represented by $C(\delta f)$. The last term on the l.h.s. indicates the nonlinear electric $\mathbf{E} \times \mathbf{B}$ drift term causing turbulent transport where $\{,\}$ denotes the Poisson brackets and Φ denotes elctrostatic potential averaged over the gyromotion. Collective motions of ions described by gyrokinetic equation change the fluctuating electric field. The perturbed ion distribution function δf is substituted into the quasi-neutrality condition of space charge for calculation of the electrostatic potential fluctuations where the adiabatic electron response is assumed (except for the zonal flow component). Toroidal flux tube coordinates *(x,y,z)* are employed where y and z are defined in terms of the poloidal angle θ, toroidal angle ζ and the safety factor q as $y = (r_0 / q_0)[q(r)\theta - \zeta]$ and $z = \theta$. Flux-surface label r is defined by toroidal flux $\Psi_T = \pi B_0 r^2$ while radial coordinate is $x = r - r_0 \ (\ll r_0)$ where r_0 `represents minor radius at which local background parameters are evaluated and $q_0 = q(r_0)$.

Effects of the helical confinement field are introduced through variation of the magnetic field strength $|\mathbf{B}|$ along the field line, such that

$$B = B_0 \left\{ 1 - \epsilon_{00}(r) - \epsilon_t(r)\cos z - \sum_{l=L-1}^{l=L+1} \epsilon_l(r) \cos\left[(l - Mq_0)z - M\alpha \right] \right\} \qquad (2.2)$$

where $\epsilon_l(r)$ denotes amplitude of a helical component with the poloidal period number l. The major helical field of the LHD is given by $L = 2$ and $M = 10$ where L and M mean the poloidal and toroidal period numbers of the confinement field, respectively. The main helical field is ϵ_L while the side-band components and the average normal curvatures are given by ϵ_{L-1}, ϵ_{L+1} and $\epsilon'_{00} = d\epsilon_{00}/dr$, respectively. For the tokamak configuration $\epsilon_l = 0$. The field-line label is denoted by α and is set to *0* in Eq. (1.2) since both the linear ITG instability and the zonal-flow response depend weakly upon α. Equation (2.2) is substituted into the magnetic drift $\mathbf{v}_d$ and the mirror force term (the last term in the square brackets on the l.h.s. of Eq.(2.1). A more detailed account of the GKV simulation model may be found in Ref. [11].

3. Simulation results

In the present study, the nonlinear GKV simulation implemented with the specified magnetic field parameters successfully confirms generation of large zonal flows enough to reduce the ion heat transport in the inward-shifted plasma. The obtained results are consistent with an experimental observation of better confinement in the inward-shifted LHD plasma [8]. Color contours of the flux-surface averaged electrostatic potential ϕ in the steady ITG turbulence are presented in Fig. 1. The ballooning-type mode structure of the ITG instability observed in the linear growth phase is destroyed in the latter turbulent state by the self-generated zonal flows. For the inward-shifted configuration shown in Fig. 1 (right), we see clear structures of poloidal zonal flows in the potential profile mapped on the poloidal cross section, while more isotropic vortices are observed in the standard case, also seen in this Figure (left).
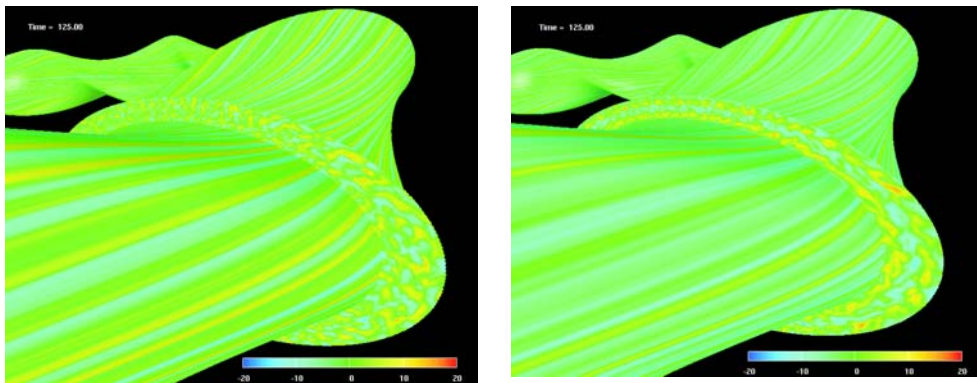

Fig. 1 Color contours of the electrostatic potential ϕ of the zonal flow and the ITG turbulence obtained by the GKV simulation for the standard (left) and the inward-shifted case (right) LHD configuration at $t = 120 L_n / v_{ti}$. Values of electrostatic potential are normalized to $e\phi L_n / T_e \rho_i$.

Spatiotemporal profiles of the zonal flows in two configurations and in the tokamak case are shown in Fig. 2 with spatial coordinate corresponding to the radial position. Zonal flow potential was generated at 2500 time points (from $t = 60\, to\, 250\, L_n / v_{ti}$), and at 130 radial positions. Peak amplitude of the time-averaged zonal-flow potential for the inward-shifted plasma is about six times larger than the largest amplitude of the standard case.
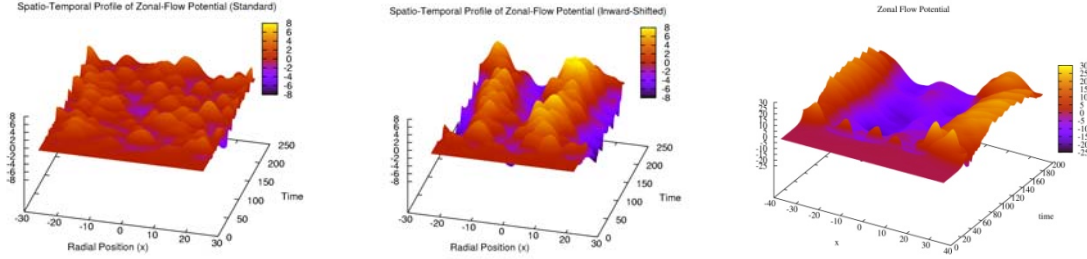

Fig. 2 Spatiotemporal profiles of the electrostatic potential ϕ of the zonal flow obtained by the GKV simulation for the standard LHD (left), the inward shifted LHD (center) and the tokamak configuration (right). Normalization is the same as in Fig. 1.

A brief inspection of the spatiotemporal patterns for two configurations reveals more spatially ordered and more energetic coherent structures in the inward-shifted case while in temporal domain this distinction is somewhat less pronounced.

4. Analysis of spatiotemporal plasma dynamics

The dynamics $\phi(x,t)$ is decomposed in terms of spatial and temporal eigenmodes

$$\phi(x,t) = \sum_{n=1}^{N} A_n \varphi_n(x)\psi_n(t), \qquad (4.1)$$

where the eigenvalues A_n are ordered in a decreasing sequence $A_0 \geq A_1 \geq ... > 0$. Eigenfunctions $\varphi_n(x)$ are eigenfunctions of the spatial two-point correlation operator U^*U, where U^* represents the complex conjugate of U, while $\psi_n(t)$ are eigenfunctions of the temporal two-point correlation operator UU^*. The kernel of U is the spatiotemporal dynamics of $\phi(x,t)$ itself. The eigenvalues of these two operators are equal to A_n^2. The method [14],[15] allows immediate evaluation of the number of degrees of freedom of the spatiotemporal dynamics, which is defined as the smallest number of modes necessary to describe $\phi(x,t)$ and is also referred to as the global dimension of $\phi(x,t)$. Since the spectral decomposition of U is generated directly from the dynamic system $\phi(x,t)$ the eigenfunctions and the eigenvalues of the operator U contain information on the attractor of the dynamics and the number of nonzero eigenvalues of the operator U represents the dimension of the smallest linear subspace containing the attractor. The global energy of the

spatiotemporal signal $\phi(x,t)$ is expressed as the sum of energies of dominant coherent structures which correspond to nonzero eigenvalues, i.e.

$$E(\phi) = \sum_{x,t} \phi(x,t)^2 = \sum_{n=1}^{N} A_n^2 \qquad (4.2)$$

.

In Fig. 3 the eigenvalues A_n^2 (corresponding to the energy content of modes numbered from *1 to N*) are presented for the helical configurations (standard (left) and inward shifted (center)) and for the tokamak (right). It is evident that in the standard configuration the energy is distributed among eight dominant modes (zonal flows) with almost monotonic decrease of energy with the mode index. For the inward shifted case most of the energy is contained in the
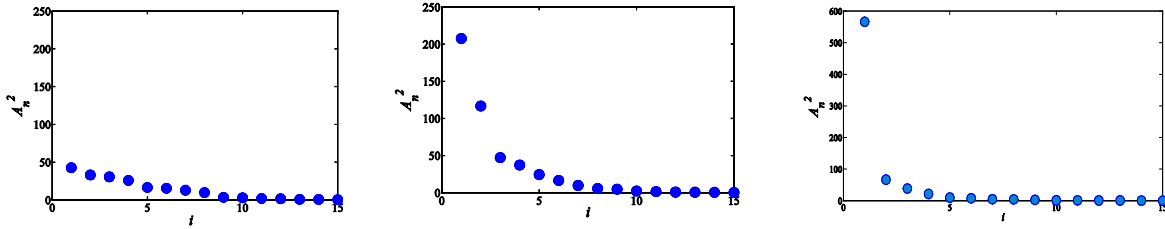

Fig. 3 Non-zero eigenvalues of the bi-orthogonal decomposition for the standard helical (left), the inward shifted configuration (center) and the tokamak (right). i denotes sequential number of an eigenvalue.

first two modes (68%) with the first mode carrying 43% of the total energy. The total energy of the inward shifted configuration is 2.5 times larger than the total energy of the standard configuration and it is striking that the main difference between the energy content of two configurations comes from the large energy accumulation in the first two modes of the inward shifted case. Employing the criterion presented in [16] it may be inferred that the global dimension the zonal flow dynamics in the standard configuration is *8,* in the inward shifted case *4,* and in this particular tokamak case *3*. The low dimensionality of the inward shifted configuration dynamics is remarkable and shows that the parameters modelling the helical configuration, namely the safety factor, the magnetic shear parameter, the inverse aspect ratio, the field strength and their radial derivatives, act as a set of control parameters for spatiotemporal chaos suppression and in general for control of chaos. In Figs. 4 and 5 the first four spatial eigenfunctions of the spatiotemporal dynamics in all cases considered here are presented.
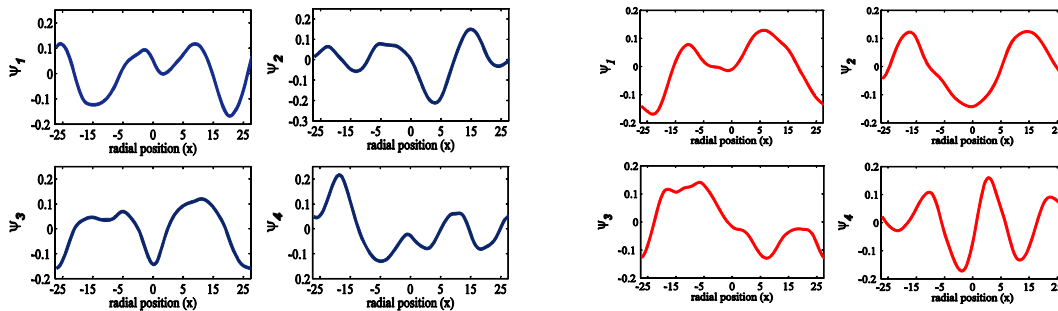

Fig. 4 First four eigenfunctions of the bi-orthogonal decomposition for the standard configuration (left), the inward shifted configuration (right) and the tokamak case (below).
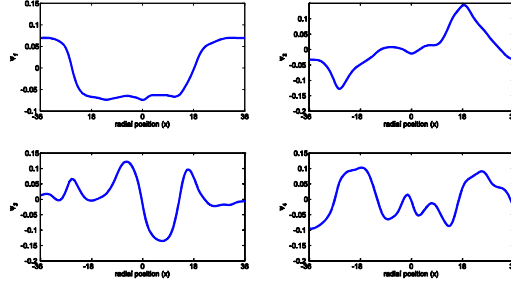
Fig. 5 First four eigenfunctions of the bi-orthogonal decomposition for the

It may be immediately noticed that the modes of the inward shifted configuration are more regular while even modes ψ_2 and ψ_4 are almost sinusoidal with an evident symmetry around the central radial position (middle of the spatial axis). In order to gain deeper understanding of spatiotemporal dynamics we extract the Lyapunov spectrum (LS) for $\phi(x,t)$ where LS is the set of Lyapunov exponents $\{\lambda_i\}_{i=1}^{N}$ arranged in decreasing order. The estimation is performed using a pure spatial reconstruction with increasing spatial embedding dimension d_s. The spectrum is then used to obtain the dimension of the chaotic attractor (the number of effective degrees of freedom) which is given by the so called Lyapunov dimension [17]

$$D_L = j + \frac{1}{|\lambda_{j+1}|}\sum_{i=1}^{j}\lambda_i, \tag{4.3}$$

where j is the largest integer for which $\sum_{i=1}^{j}\lambda_i > 0$. D_L is a global quantity defined for the whole system. One may also determine the Kolmogorov-Sinai (KS) entropy h from the LS using the following approximation [18]

$$h = \sum \lambda_i^{+}, \tag{4.4}$$

where the summation is over positive Lyapunov exponents λ_i^{+}. The KS entropy quantifies the mean rate of information generation in a system (the mean rate of uncertainty increase due to infinitesimal perturbations). For spatiotemporal chaotic systems both D_L and h are extensive quantities (i.e. D_L and h increase linearly with the system size). In Fig. 5 the sum of Lyapunov exponents $\sum_{k=1}^{i}\lambda_k$ is presented as a function of I for various sizes of the system. From this representation the Lyapunov dimension may be readily obtained from the intersection with the horizontal axis and the KS entropy is determined from the maximum of the curve. It may be easily noticed that both the Lyapunov dimension and the KS entropy of the standard shifted configuration (left, blue curves) are always greater than the D_L and h of the inward shifted one (red curves). A closer inspection of this Figure reveals that both D_L and h are extensive quantities. Hence, the standard configuration is more chaotic with the greater number of effective degrees of freedom and the mean rate of information production is

higher in the standard configuration. A direct consequence of this property has a powerful impact on transport properties and points to the deep relationship between Lyapunov exponents and transport properties of confined plasma system
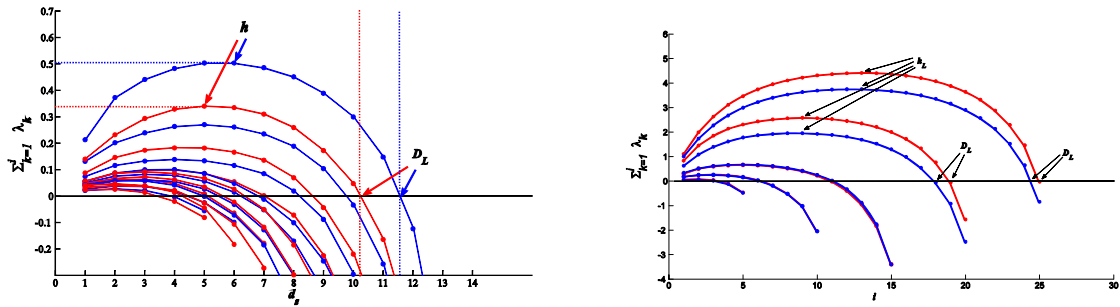

Fig. 5 The sum of Lyapunov exponents as a function of the system size d_s for the helical configuration (left) and the tokamak (right). For the helical configuration standard configuration dynamics is shown in (blue) and inward shifted dynamics in (red). For the tokamak blue and red colors denote clockwise and counterclockwise spatial directions from $\phi = 0$. The Lyapunov dimension D_L and the Kolmogorov-Sinai entropy h may be estimated from the diagrams.

Further comparison between the dynamics solely in the temporal domain may be obtained by using the recurrence plot (RP) analysis of time series [19], [20] which offers remarkable visual difference between temporal patterns. For this purpose we use temporal variations of electrostatic potential at the central spatial (radial) position i.e. $\phi = 0$. Using standard methods to embed the time series we obtain the recurrence plots shown in Fig. 6 for the standard (left), the inward shifted (center) and tokamak configurations respectively[1]. Recurrence plot for the standard configuration reveals irregular diagonal areas (lines) parallel to the main diagonal with sparsely distributed horizontal and vertical areas (lines) which indicate deterministic chaos. In contrast RP of the inward shifted configuration displays dominant horizontal and vertical areas which mark time periods during which state does not change or changes very slowly, a sign of lesser chaotic state (intermittency).
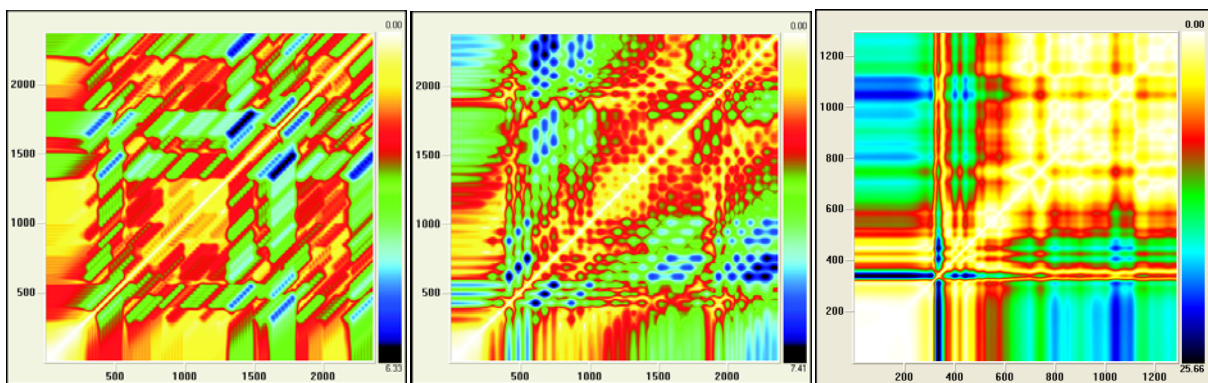

Fig. 6 Recurrence plots of time series $\phi(t, x = 0)$ \recorded at the central radial position. Standard configuration case is on the left, the inward shifted in the center and tokamak case on the right.

---

[1] Recurrence plots were generated using Eugene Kononov's Visual Recurrence Analysis software (www.myjavaserver.com/~nonlinear/vra)

Intermittency is also dominant dynamics in the tokamak configuration. The time series of $\phi(t, x = 0)$ for the standard configuration has two positive Lyapunov exponents indicating hyper chaos while for the inward shifted and the tokamak case only one.

5. Conclusion

The nonlinear GKV simulation substantiates generation of zonal flows capable of reducing ion heat transport in the inward-shifted configuration of a helical system. The nonlinear GKV equation for the perturbed ion gyrokinetic distribution function in the low-β electrostatic limit is solved as a partial differential equation defined in the five dimensional phase space. Simulation results reveal enhanced zonal flow generation and larger amplitude of these coherent structures in the inward-shifted configuration accompanied by lower ion thermal diffusivity. An analysis of electrostatic potential dynamics performed with the use of methods of nonlinear dynamics systems theory and the theory of chaos shows that both the helical (standard and the inward-shifted configurations) and the tokamak exhibit extensive properties characteristic of spatiotemporal chaos. A considerable reduction of spatiotemporal chaos is evident in the inward-shifted configuration accompanied by generation of more energetic zonal flows in comparison with the standard case. Since the set of parameters comprising of the safety factor, the magnetic shear parameter, the inverse aspect ratio, the magnetic field strength and their radial derivatives models helical configuration and hence controls chaotic dynamics, insight into their interplay in the chaos control process may open up new possibilities for efficient control of spatiotemporal chaos.

References

[1]   M. N. Rosenbluth and F. I. Hinton, Phys. Rev. Lett. **80** (1998) 724.
[2]   P. H. Diamond, S.-I. Itoh, K. Itoh and T. S. Hahm, Plasma Phys. Control. Fusion **47** (2005) R35.
[3]   A. Fujisawa et al, Phys. Rev. Lett., 93 (2004) 165002.
[4]   Z. Lin et al, Science **281** (1998) 1835.
[5]   N. Winsor, J.L. Johnson, J.J. Dawson, Phys. Plasmas **11** (1968) 2448.
[6]   H. Sugama and T.-H. Watanabe, Phys. Rev. Letters **94** (2005) 115001.
[7]   H. E. Mynick, Phys. Plasmas **13** (2006) 058102.
[8]   H. Yamada et al, Plasma Phys. Control. Fusion **43** (2001) A55.
[9]   H. Sugama and T.-H. Watanabe, Phys. Rev. Letters, **94** (2005) 115001.
[10]   H. Sugama, and T.-H. Watanabe, Physics of Plasmas, **13** (2006) 012501.
[11]   S. Ferrando-Margalet, H. Sugama, and T.-H. Watanabe, Physics of Plasmas **14**(2007) 122505.
[12]   T. -H. Watanabe, H. Sugama and S. Ferrando-Margalet, Phys. Rev. Lett. **100** (2008) 195002.
[13]   M. Rajković, T. -H Watanabe, M.M. Škorić, Physics of Plasmas **16** (2009) 092306.
[14]   N. Abry and R. Guyonnet and R. Lima, J. Stat. Phy.,**64** (1991) 683.
[15]   M. Skoric, M. Jovanovic and M. Rajkovic, Phys. Rev. E **53** (1996) 4056.
[16]   M. Rajkovic, Physica A **287** (2000) 383.
[17]   J. L. Kaplan and J. A. Yorke, Lecture Notes in Mathematics, Springer, New York, **730** (1979) 204.
[18]   J. -P. Eckmann and D. Ruelle, Rev. Modern Phys., **57** (1985) 617.
[19]   J. -P. Eckmann, O. Kamphorst and D. Ruelle, Europhy. Lett. **5** (1987) 973.
[20]   N. Marwan, M. C. Romano, M. Thiel and J. Kurths, Phys. Reports **438** (2007) 237.